

Tectonic-Sedimentary Evolution of Piedra Clavada and Koluel Kaike Fields, Golfo San Jorge Basin, Santa Cruz Province, Argentina*

Ariel Schiuma¹, Carolina Crovetto¹, Adrián Rasgido¹, and Ornella López Alvarado¹

Search and Discovery Article #20210 (2013)

Posted October 18, 2013

*Adapted from extended abstract prepared in conjunction with poster presentation at AAPG International Conference and Exhibition, Cartagena, Colombia, September 8-11, 2013, AAPG©2013

¹Pan American Energy LLC, Av. Leandro N. Alem 1180, C1001AAS, Buenos Aires, Argentina (aschiuma@pan-energy.com)

Abstract

The Piedra Clavada and Koluel Kaike fields are located in the south flank of Golfo San Jorge Basin, Argentina, where the basin has an extensional behavior with principal faults of NW-SE strike. The source rock is the Pozo D-129 Formation, and the main reservoirs belong to the Cañadón Seco Formation and in a lower proportion of the Mina del Carmen Formation. This study was performed to better understand the potential of this last Formation.

Based on seismic character and electrical response of well-logs, the top and base of the Mina del Carmen Formation (MdC) were established, defining three sub-units named MdC-A, MdC-B and MdC-C from base to top. Structural and isochoric maps were generated. Seismic attributes were computed to identify the paleofluvial systems, representing the principal reservoirs. To determine the tectonic control on the sedimentation, the kinematical behavior of the principal fault was analyzed by computing the vertical throw for each of the interpreted horizons along the fault strike.

Isochoric maps and fault displacement graphics allowed us to define the paleogeomorphological framework, identifying the paleohighs and the paleolows. The principal fault is composed of several segments which have been linked during its evolution, serving as access paths for sediments from the footwall to the hanging wall. Two logfacies were identified by analyzing the well logs: a coarse logfacies (CLF) and a fine one (FLF). Logfacies proportions were computed in every sub-unit, allowing us to qualitatively infer the amount of sediments supply.

During the deposition of MdC-A, the fault presented moderate activity; there were several small depocenters in the hanging wall, and sediments reached them through the relay ramps flowing parallel to the fault strike. The highest fault activity took place during MdC-B deposition, generating a large accommodation space with more integrated depocenters. Sediments continued entering through the relay ramps,

especially those located in the eastern and western fault tips, and were transported parallel to the fault strike to the depocenters. Finally, during the deposition of MdC-C, the fault activity ceased and accommodation space was generated by thermal subsidence. Therefore, sediments were carried to the north towards the basin depocenter.

These changes in the paleomorphological framework conditioned the placement of reservoirs within MdC Formation. This study will allow us to identify the locations for future drilling prospects.

Introduction

The Piedra Clavada and Koluel Kaike fields are mature oil fields located in the southern flank of Golfo San Jorge Basin, Patagonia, Argentina, covering an area of approximately 290 square kilometers ([Figure 1](#)). They have been developed since 1960, mainly from the Upper Cretaceous Cañadón Seco Formation and less from the Albian Mina del Carmen Formation.

Both fields are divided in two blocks by a principal east-west striking, north-dipping rift fault, with throw values ranging from 100 m to more than 800 m in the deepest sections. The principal reservoirs are located in the roll-over anticline generated in the hanging wall, where the fault served both as the migration path and a present-day seal for the hydrocarbons. In the footwall, some shallow reservoirs exist with lower production from both formations.

This principal fault behaved as an important tectonic control for the fluvial systems of Mina del Carmen Formation because of its sedimentary activity. Mina del Carmen Formation is a fluvial succession with reservoirs mainly composed by tuffaceous sandstones of 3-10 m thickness (Foster and Iovine, 2008; Scazzioti, 2008) and diagenetically altered tuff successions associated to the development of standing bodies of waters in floodplain environments (Acuña et al., 2011); floodplains composed by fine volcanic ash constitute the seal of the petroleum system. The reservoirs generally present 14% average porosity and permeability ranging from 50 to 200 mD, requiring hydraulic-fracture stimulation to be economically profitable. This fact has prevented this formation from being highly developed until now, when production from traditional reservoirs from Cañadón Seco Formation are declining and other resources must be taken into account.

The present study was intended to gain an understanding of the depositional model of Mina del Carmen Formation and the characteristics of its reservoirs, and to identify the potential areas to place future drilling prospects.

Geological Setting

The Golfo San Jorge Basin is an intracratonic basin originated during Gondwana's break-up. It was opened by a discontinuous extensional regime with several reactivation phases from the Late Jurassic to Early Miocene (Uliana and Biddle, 1987; Barcat et al., 1989; Figari et al., 1999). Its stratigraphic column is shown in [Figure 2](#).

During the Jurassic, the extension created NW-SE to E-W oriented grabens and half-grabens which were filled with proximal volcanics and volcanoclastics deposits (Pankhurst and Rapela, 1995; Pankhurst et al., 1998). During the Lower Cretaceous there was a shift in the location of

the active extension zone, generating a depocenter oriented sub-perpendicular to the continental margin that had begun to appear (Uliana et al., 1989; Fitzgerald et al., 1990).

The Golfo San Jorge Basin is divided into five major regions, according to its structural style (Figari et al., 1999). In the three Eastern regions (North Flank, Basin Centre and South Flank), an extensional style prevails (Fossa-Mancini, 1932; Giacosa et al., 2004; Foix et al., 2008, 2012). To the west, NNW-SSE striking thrust and folds compose the San Bernardo Fold Belt, formed by Tertiary tectonic inversion of normal faults (Homovc et al., 1995). The Western Sector, located further west of the Fold Belt, is dominated by extensional structures (Clavijo, 1986) with little evidence of positive tectonic inversion (Figari et al., 1996).

During the synrift stage, in the Neocomian, Pozo Anticlinal Aguada Bandera and Pozo Cerro Guadal formations were deposited, consisting of lacustrine successions up to 2200 m thick. Following that, the Chubut Group (Chubutian Megasequence) was deposited, formed by a continental volcanoclastic succession up to 7000 m thick in the Basin Centre (Sciutto, 1981; Hechem et al., 1990; Hechem and Strelkov, 2002). During its sedimentation, several tectonic mechanisms took place, such as the reactivation of previous normal faults, an independent event with WNW-ESE to E-W striking normal faults in the Eastern Sector (Uliana et al., 1989; Chelotti, 1997), and regional subsidence during the Upper Cretaceous (Fitzgerald et al., 1990).

The Chubut Group is integrated at its base by the Barremian to Aptian Pozo D-129 Formation, a lacustrine succession, and its laterally equivalent the fluvial Matasiete Formation in the western sector. Black shales from Pozo D-129 Formation constitute the principal source rock of the basin. It is overlaid by the Albian Mina del Carmen Formation (or by the laterally equivalent Castillo Formation at basin boundaries), a fluvial to lacustrine succession constituted by reworked pyroclastic fragments (Lesta, 1968; Lesta and Ferello, 1972), with predominance of tuffaceous shales with thin interbedded tuffaceous sandstones. They are covered by a fluvial succession called the Bajo Barreal Formation, equivalent to Cañadón Seco and Meseta Espinosa formations in the South flank and Comodoro Rivadavia and Yacimiento El Trébol formations in the North flank (Figari et al., 1990; Rodriguez, 1992; Umazano et al., 2008). These Formations are stacked sequences of sandstones and shales, with minor volcanoclastic material; sands are deposited as alluvial fans, braided and meandering fluvial systems.

During the Tertiary, the basin was a wide tectonic depression with little subsidence, influenced by sea-level fluctuations in a passive-margin, with alternating marine and continental sedimentation (Uliana and Biddle, 1987; Legarreta et al., 1990; Legarreta y Uliana, 1994). The marine Salamanca Formation and the continental Rio Chico Formation were deposited during the Paleocene, followed by Sarmiento Formation, Patagonia Formation and Santa Cruz Formation in the rest of Cenozoic; glaciofluvial gravel strata of Plio-Pleistocene age complete the basin filling (Paredes, 2009).

Data and Methodology

Seismic Data

The Piedra Clavada and Koluel Kaike fields are both covered with 3D seismic surveys, registered in 1994, 1995 and 2005. Seismic data was acquired employing Vibroseis sources, processed and reprocessed in 2005 independently, with standard methodologies. The frequency ranges

between 8 to 70 Hz with a dominant frequency of 30-35 Hz in most of the area, giving a vertical resolution which ranges from 10 m to 40 m according to depth; the spatial resolution is approximately the bin size: 25 m for Koluel Kaike Field and 30 m for Piedra Clavada Field.

The tops of all formations were identified and carefully interpreted in both fields, with special emphasis in highly structured areas. In particular, the Mina del Carmen Formation (MdC) was divided in three different sub-units, according to their seismic character and electrical response in well logs ([Figure 3a](#)). The lower sub-unit, named MdC-A, is characterized by chaotic and highly discontinuous reflectors, with high amplitude at the top. The following sub-unit, MdC-B, is the thickest, with moderate to high amplitude continuous reflectors. The upper sub-unit, MdC-C, is highly discontinuous with low to moderate amplitude reflectors.

The seismic division of Mina del Carmen Formation is replicated in the electrical response of the well logs ([Figure 3b](#)). The top of the formation shows an elevation in gamma ray values from a background of $\sim 70^\circ\text{API}$ to $\sim 80\text{-}90^\circ\text{API}$, and the resistivity logs increase their background from $\sim 1.5\text{ ohm.m}$ to $\sim 2.5\text{ ohm.m}$ (maximum is 20 ohm.m), coincident with the volcanoclastic material apparition in the geologic record. MdC-B top shows an extra increase in the background values of resistivity to 3.5 ohm.m , with peaks higher than 10 ohm.m , and gamma ray shows an increase in its background to 100°API . MdC-A top shows a big kick in gamma ray log, growing its background to 120°API . Pozo D-129 Formation top is characterized by oolitic limestones deposited along the coast of the lake, with a decrease of gamma ray and an increase in resistivity.

Structure

Fifty one wells with measured sonic and density logs, and some with borehole seismic data (checkshots or VSP), were calibrated to obtain detailed time-depth functions in each location. A velocity model for the survey was built employing those functions and the interpreted horizons to guide the interpolations. This model allowed time-to-depth conversion of horizons in order to build structural and isochoric maps.

From the horizon interpretation and the velocity model, structural and isochoric maps were built for all the sub-units. A structure map at top of the Mina del Carmen Formation can be seen in [Figure 4a](#).

The hanging wall is characterized by a roll-over anticline with a complex fault system in both fields ([Figure 4b](#)). Structure deepens towards the north, to the basin center. The footwall has been less affected by tectonic activity, and its structure is smoother with low slope. There is an important en-echelon fault system produced by a basement fault placed at the middle of the footwall block in Koluel Kaike Field, synthetic to the principal fault, and probably with a common origin, representing one of the last steps in the basin which ends southwards.

The eastern sector of Koluel Kaike is characterized by the intrusion of an ultrabasic igneous rock, approximately 300 m thick, located at 1200 m depth next to the Top of Mina del Carmen Formation. This body was placed during the Tertiary, like many others in the basin, elevating the upper sequence of the Cañadón Seco Formation. The evaluation of this area is not easy because this ultrabasic rock generates a large distortion in the seismic image, but with the help of well data and regional structural information, it is possible to infer that the fault tip is placed toward the east of the field, and might be relayed by another synthetic fault at the northeast of the neighboring area. Both rift faults could have been

linked by perpendicular minor faults generating a Rider structure, a weakness zone which could have favored the ascension and placement of the intrusive rock.

Kinematical Analysis of the Principal Fault

In extensional systems, normal faults create asymmetrical accommodation space and control sediment deposition (Leeder and Gawthorpe, 1987; Prosser, 1993; Alexander et al., 1994; Contreras et al., 2000; Gawthorpe and Leeder, 2000); understanding the process of fault growth allows us to understand the sedimentary response. Seismic reflection data sets can be very helpful for this purpose, as shown in several studies (Willemse et al., 1996; Morley, 1999; Dawers and Underhill, 2000; Morley, 2002a, 2002b; McLeod et al., 2002; Baudon and Cartwright, 2008; Lohr et al., 2008; Paredes et al., 2013)

Throw (or displacement) measurements along fault planes can be easily performed from available 3-D seismic datasets, measuring the current throw of selected seismic horizons in regularly spaced lines, perpendicular to the fault surface. Interval displacements (or throw graphics) and isothrow contour maps can be obtained with this technique (Morley et al., 2004, 2007). Paleorelief, changes in the location and shape of depocenters, and changes in the number of extensional phases that occurred during deposition of the involved sedimentary sequence can be inferred from them.

In our study, throw fault values were systematically measured on the principal rift fault of both fields using seismic lines oriented orthogonal to fault strike with a spatial separation between consecutive lines of 125-150 meters depending on the bin size. This was performed computing the time where horizons intersect with the fault plane in the footwall and in the hanging wall, and calculating their difference. Horizons corresponding to the top of Mina del Carmen Formation and its sub-units, and the Pozo D-129 Formation and two intra-formation horizons (D129I3 and D129I6) were employed in the calculation. To simplify the analysis, and due to the excellent well control, throws were just expressed in values of two-way travel time (TWT) and not converted to depth. Vertical throw was used as an approximation of fault displacement.

The computation of the intersection time between horizons and the fault plane is sometimes uncertain in the hanging wall, due to the fault's system associated with the principal fault. Secondary faults impose additional throws to the final diagram, making the interpretation more difficult. Considering this, times for the hanging wall were measured in the footwall of the principal antithetic fault ([Figure 5b](#)). Although not strictly correct, the throw diagram so obtained ([Figure 5a](#)) shows results consistent with the ones revealed by the isochoric maps.

The vertical throw versus distance diagram ([Figure 5a](#)) shows that the principal fault is composed of three different segments, linked during its evolution until its present shape as a single fault. There are two main depocenters, one in the middle of Koluel Kaike Field and the other between the fields. Both depocenters were active during deposition of the upper portion of Pozo D-129 Formation and MdC-A and MdC-B sub-units; this syn-sedimentary activity is reflected by the difference in throw for two consecutive horizons. During deposition of MdC-C the fault ceased its activity, reflected by equivalent throw for MdC-B and MdC-C horizons (Crovetto et al., 2013). By the end of the Cretaceous, after deposition of Chubut Group, a new extensional phase took place in the basin during the marine ingression of the Salamanca Formation, reflected in the present day throw values. These results concerning periods of activity agree with those observed for the North Flank of the

Cuenca San Jorge Basin (Cayo et al., 2011; Paredes et al., 2013), and complete the preliminary results shown for Koluel Kaike Field (Crovetto and Schiuma, 2013).

In the eastern area of Koluel Kaike Field fault throw decreases, but the presence of the intrusives makes the identification of the fault tip not possible. In the middle of this field, a narrow depocenter is formed (29 km) beside a relay ramp where the throw decreases (27.5 km). In Piedra Clavada Field the activity decreases to the west, where the fault tip is identified in the neighbor field, and a synthetic relay fault begins to grow at the north of the principal. There is an important relay ramp in the middle of the Piedra Clavada (13 km), with higher activity in the eastern segment, the one responsible for the large depocenter in the area between the fields (22 km). The tectonic activity in Piedra Clavada is in general lower than in Koluel Kaike Field, but periods of activity are coincident.

Seismic Attributes

Seismic attributes were computed for both seismic datasets and all the sub-units of Mina del Carmen Formation to help in interpreting the depositional environment (Chopra and Marfurt, 2007). RMS amplitudes were extracted in windows of 10-20 ms, covering the entire Formation (Brown, 2004). Spectral decomposition in frequencies of 20, 25, 30 and 35 Hz was also performed, with calculation windows of 64 ms, using RGB blending of three frequencies to enhance the visualization (Partyka et al., 1999).

The best images are achieved in the footwall, where the seismic resolution is higher due to its lower depth and little structuration. Several aspects of Mina del Carmen fluvial systems were identified, such as straight channels and several meandering channels with well-developed point bars. Flow directions are mainly north-northeast, with some wandering channels in the footwall where there was very low paleorelief. As an example of visualization, [Figure 6](#) shows the RGB blending of 20, 25 and 30 Hz corresponding to the Top of Mina del Carmen Formation; several channels can be identified in the footwall and in the hanging wall of both fields, with high or low amplitudes, and N-NE directions perpendicular to the fault. Some channels crossing the fault can be also identified.

Logfacies Identification and Distribution

Information from 98 wells was taken into account for this study, all of them reaching at least the top of MdC-A sub-unit. There are no wells crossing the full stratigraphic column in Piedra Clavada Field because the structure greatly deepens towards that area and it has not been drilled yet. Thus, logfacies analysis was only performed for Koluel Kaike wells. All these wells have Spontaneous Potential, Deep and Shallow Resistivity logs, and most of them have Density Porosity and Neutron Porosity logs.

With this information, two logfacies were identified: a coarse and a fine logfacies ([Figure 7](#)). The coarse logfacies is composed of fluvial deposits, mainly channel fillings and bars, with porosities above 10% and SP lectures below -10 mV. Fine logfacies are the typical floodplains of these fluvial systems and behave as the classical seals for the petroleum system. They show SP values above -10 mV and porosities below 12%.

The coarse/fine logfacies ratio was calculated for each sub-unit, for the hanging wall and the footwall independently. In MdC-A ([Figure 8a](#)), this ratio is 0.18 in the hanging wall, 0.18 in the footwall near the fault and 0.26 in the south. In MdC-B ([Figure 8b](#)), the ratio's values are 0.17 in the hanging wall, raising to 0.39 in the footwall near the fault, and decreasing to 0.17 in the southern part of the footwall. In MdC-C ([Figure 8c](#)) the ratio has values of 0.15 in the hanging wall, goes up to 0.38 in the footwall near the fault trace and is 0.35 in the southern part of the study area.

Discussion

By integrating results from seismic isochoric maps, channels identified through seismic attributes, logfacies ratios and the principal fault kinematical analysis, a gross depositional map for each sub-unit was interpreted. MdC-A sub-unit isochoric map ([Figure 9](#)) shows thickness variations between the footwall and the hanging wall, reflecting the fault activity, coincident with the result of fault displacement diagrams ([Figure 5](#)). The fault activity generated accommodation space in the hanging wall, where deposits show a wedge shape towards the fault.

The footwall had two elevated areas which served as barriers for the water drainage. In the southern part of Koluel Kaike, the fluvial systems flowed to a depocenter, acting as a base level, placed at the south of the field, identified through old 2D seismic lines. From the high topographic area, drainage in Koluel Kaike was to the north-northeast towards the principal fault; this agrees with channels identified using seismic attributes, which showed a north-northeast direction. When channels reached the fault scarp proximity in the footwall, they are supposed to have adopted a sub-parallel direction until they reached a relay ramp, through which sediment flux was then driven from the footwall to the hanging wall. The identified relay ramps were placed in the middle of each field and in both extremes, with minimum throw values in displacement graphics ([Figure 5](#)). An argument for this is the fact that there is no evidence of conglomeratic deposits in the hanging wall which could be due to alluvial fans of sediments cutting and crossing the fault scarp. Sediments in the hanging wall show the same grain size as in the footwall, revealing that the transport agent energy was similar in both cases. Other evidence that detritus flux was through relay ramps is that the coarse/fine logfacies ratio is larger in the proximity of them, and decreases in the distal area. Once in the hanging wall, water flumes flowed parallel to the fault scarp until reaching the depocenters; logfacies ratios show that sedimentation of coarse grained material took place in a narrow corridor near the fault scarp. Finally, depocenters are supposed to be filled with fine grained material, although not drilled.

During the deposition of MdC-B sub-unit ([Figure 10](#)), the principal fault had a higher activity, as showed by the displacement diagrams ([Figure 5](#)) and the larger difference in the sub-unit thickness between footwall and hanging wall. Thus the main depocenter in the hanging wall grew, integrating previous disperse depocenters and becoming a larger and unique local base level, controlling all the sediment flux. In the footwall, paleohighs were still the highest topographic zones in the area, so they still controlled the fluvial system's directions. From the footwall to the hanging wall, sediments were again led through the relay ramps. As the depocenter was wider, the sedimentation was parallel but not restricted to the portion next to the fault surface, covering a wider area away from it, as observed in reservoir logfacies.

Regarding the accommodation space, both sub-units MdC-A and MdC-B behaved similarly, although during the deposition of the second one more space was generated. There was also a difference in sediment supply for both sub-units. In the footwall, MdC-A shows a higher coarse/fine logfacies ratio in the proximities of the high relief area (0.26), being this a deposition zone, while in the surroundings of the fault this proportion decreases to 0.18, behaving as a bypass area of sediments going to the hanging wall. In MdC-B sub-unit this ratio is inverted,

with a lower proportion of coarse/fine logfacies near the high topographic area (0.17), and a larger proportion next to the fault plane (0.39). This situation could be due to the variation in the location of the high topographic area; for MdC-A the highest area was placed at the south of the wells where logfacies were identified, and the change in slope could have been enough to allow deposition of coarse material. In MdC-B sub-unit, the highest area coincided with the present location of the wells, probably acting as a sediment supply area more than a depositional area. Another cause could have been an increment of sediment supply due to an increment of the amount of water entering the system, generating a more competent flux in the higher areas with less deposition, but greater deposition in the lower areas near the fault scarp. In the hanging wall, the coarse/fine logfacies ratio remains stable in both sub-units (0.18). Taking into account that the fault activity was higher during MdC-B, the sediments supply should have been larger to maintain this relation. Nevertheless, climate changes and sediment supply analysis were not part of the objectives of this contribution, so further work should be done in order to verify or reject this hypothesis.

When deposition of sub-unit MdC-C took place ([Figure 11](#)), fault activity had already stopped ([Figure 5](#)); sub-unit thicknesses are almost the same in both footwall and hanging wall. In the southern part of the footwall, the paleohigh area still persisted, controlling the footwall deposits. As the fault surface did not represent a barrier any more, the relay ramps were no longer the entrance areas for the sediment from the footwall to the hanging wall. Sediment flux crossed perpendicular to the fault strike, as showed in spectral decomposition of the seismic data ([Figure 6](#)). Fluvial systems flowed from the south to the north, controlled by a larger base level located at the north, outside the study area. Reservoir logfacies in the hanging wall wells show more lateral variation, alternating channel stacks with floodplains, thus referring to straight channels flowing to the north in different straight paleofluvial valleys.

Concerning prospect identification, MdC-A and MdC-B show a clear tendency in sediments concentration due to their common tectonic history. In both sub-units, as faulting was active, sediments entered the hanging wall from the footwall across the relay ramps. The eastern sector of the Kouel Kaike Field is the zone where the main development of Mina del Carmen Formation occurred. Today this area provides 22% of production from the Koluel Kaike Field, and has generated an increase of 30% in the proven reserves volume since the beginning of the project in 2008 (Schiuma et al., 2013). Extrapolating this idea, similar prospective areas could be all those areas linked to other relay ramps, like the one in the west side of Piedra Clavada Field, which is a mirror image of the former. This area, although not drilled yet, shows enough evidence to be similar as the proven one.

The other two relay ramps located in the middle of the fields also represent interesting prospects. A few wells drilled in Koluel Kaike beside one of them shows that coarse logfacies are present and have good production.

As MdC-C behaves differently, with no tectonic activity and sedimentation flowing perpendicular to and crossing the main fault, it is more difficult to establish the limits between fluvial paleovalleys to determine the best place to drill this sub-unit. In brief, according to our model, future wells drilled in the Mina del Carmen Formation should be directed to areas next to relay ramps where possibilities of finding more reservoirs are higher.

Conclusions

- The fields' principal fault was active during deposition of MdC-A and MdC-B sub-units, the lower and middle portions of the Mina del Carmen Formation, controlling sediment distribution in those intervals.
- During deposition of MdC-C, the upper portion of the Mina del Carmen Formation, the fault showed no activity. Sedimentation is controlled by the remaining relief and thermal subsidence of the basin, with a larger base level at the north of the fields.
- The fault is composed of three segments which linked through time, with tips located at both sides of the fields. At the western sector of Piedra Clavada Field, the fault tip is clearly identified, where other synthetic faults grow northward. At the eastern sector of the Koluel Kaike Field, the fault loses its throw but the tip is not recognizable because of the presence of intrusive igneous rock which distorts the seismic image. In spite of this, a principal fault dipping also to the north in the neighboring area allows us to state that the fault tip is under the intrusive (noisy) area.
- The different coarse/fine logfacies ratio values between the MdC-B and MdC-A sub-units in both footwall areas, and the similarity in the hanging wall, allows us to infer that there is an increase in the amount of sediments entering the system during MdC-B time. In the footwall, near the fault trace, the ratio increases in MdC-B with no change in the accommodation space between MdC-A and MdC-B. In the hanging wall, this ratio is almost equal in both sub-units, but as more accommodation space was created during the younger period, sediments influx into the hanging wall should have been higher to maintain the ratio.
- The best areas to go on with the development of Mina del Carmen Formation are those which served as relay ramps during deposition. Those are placed in the middle and eastern zones of the Koluel Kaike Field, and in the middle and western zones of the Piedra Clavada Field.

Acknowledgements

The authors are grateful to Pan American Energy LLC (PAE) for permission to publish this work.

References Cited

- Acuña, C., A. Schiuma, D. Parra, C. Droeven, M. Bernedo, and J.M. Paredes, 2011, Modelo paleoambiental de la Formación Mina del Carmen en el Yacimiento Cerro Dragón, Cuenca del Golfo San Jorge, Argentina: VIII Congreso de Exploración de Hidrocarburos, Trabajos Técnicos, p. 419- 439. Mar del Plata.
- Alexander, J., J.S. Bridge, M.R. Leeder, R.E. Collier, R.L. Gawthorpe, 1994, Holocene meander-belt evolution in an active extensional basin, southwest Montana: *Journal of Sedimentary Research*, v. 64, p. 542-559.

Barcat, C., J.S. Cortiñas, Nevistic, and H.E. Zucchi, 1989, Cuenca Golfo San Jorge, *in* G.A Chebli and L.A., Spalletti (Eds.), *Cuencas Sedimentarias Argentinas, Serie de Correlación Geológica*, v. 6, p. 319-345, San Miguel de Tucumán.

Baudon, C., and J. Cartwright, 2008, Early stage evolution of growth faults: 3D seismic insight from the Levant Basin, Eastern Mediterranean: *Journal of Structural Geology*, v. 30, p. 888-898.

Brown, A., 2004, *Interpretation of three-dimensional data*: 6th Ed. AAPG Memoir 42, 541 p.

Cayo, E.L., C.B. Crovetto, S.G. Plazibat, J.E. Stein, M.T. Diaz, and J.M. Paredes, 2011, Control tectónico sobre la sedimentación de la Formación Mina del Carmen en el Yacimiento Cerro Dragón, Cuenca del Golfo San Jorge, Argentina: 8th Congreso de Exploración y Desarrollo de Hidrocarburos, Trabajos Técnicos, p. 397-418, Mar del Plata.

Chelotti, L.A., 1997, Evolución tectónica de la Cuenca del Golfo San Jorge en el Cretácico y Terciario: algunas observaciones desde la interpretación sísmica: *Boletín de Informaciones Petroleras*, v. 49, p. 63-82.

Chopra, S., and K.J. Marfurt, 2007, *Seismic Attributes for Prospect Identification and Reservoir Characterization*: SEG Geophysical Development Series 11, 464 p.

Clavijo R., 1986, Estratigrafía del cretácico inferior en el sector occidental de la Cuenca Golfo San Jorge. *Boletín de Informaciones Petroleras*, v. 9, p. 15-32.

Contreras, J., M.H. Anders, and C.H. Scholz, 2000, Growth of a normal fault system: observations from the Lake Malawi basin of the east African rift: *Journal of Structural Geology*, v. 22, p. 159-168.

Crovetto, C., S. Plazibat, M.T. Díaz, J. Stein, E. Cayo, and J.M. Paredes, 2013, Evolución estructural y geodinámica de sistemas de fallas de la Cuenca del Golfo San Jorge: aplicaciones del método de análisis cinemático de fallas en el yacimiento Cerro Dragón: *Primeras Jornadas Geológicas de la Cuenca del Golfo San Jorge, Resúmenes en CD*. Comodoro Rivadavia.

Crovetto, C., and A. Schiuma, 2013, Análisis cinemático de la falla principal del yacimiento Koluel Kaike, flanco sur, Cuenca del Golfo San Jorge, y su rol durante la depositación de la formación Mina del Carmen. *Primeras Jornadas Geológicas de la Cuenca del Golfo San Jorge, Resúmenes en CD*. Comodoro Rivadavia.

Dawers, N.H., and J.R. Underhill, 2000, The role of fault interaction and linkage in controlling synrift stratigraphic sequences: Late Jurassic, Statfjord East area, northern North Sea: *AAPG Bulletin*, v. 84, p. 45-64.

Figari, E.G., J.J. Hechem, and J.F. Homoc, 1990, Arquitectura depositacional de las “Areniscas Verdes” de la Formación Bajo Barreal, provincia del Chubut, Argentina: 3rd Reunión Argentina de Sedimentología, v. 1, p. 130-138.

Figari, E.G., M.S. Cid de la Paz, and G. Laffitte, 1996, Neocomian half graben in the western San Jorge Basin, Argentina: petroleum systems, origin and tectonic inversion: AAPG Bulletin, v. 80, p. 1289-1290.

Figari, E., E.E. Stelkov, G. Laffitte, M. Cid de la Paz, S. Courtade, J. Celaya, A. Vottero, P. Lafourcade, R. Martinez, and H. Villar, 1999, Los sistemas petroleros de la Cuenca del Golfo San Jorge: Síntesis estructural, estratigráfica y geoquímica: 4th Congreso de Exploración y Desarrollo de Hidrocarburos, Buenos Aires., p. 197-237.

Fitzgerald, M.G., R.M. Mitchum, M.A. Uliana, and K. T. Biddle, 1990, Evolution of the San Jorge Basin, Argentina: AAPG Bulletin, v. 74/6, p. 879-920.

Foix, N., J.M. Paredes, and R. Giacosa, 2008, Paleo-earthquakes in passive-margin settings, an example from the Paleocene of the Golfo San Jorge Basin, Argentina: Sedimentary Geology, v. 205, p. 67-78.

Foix, N., J.M. Paredes, and R.E. Giacosa, 2012, Upper Cretaceous-Paleocene extensional phase in the Golfo San Jorge basin (Argentina): growth-fault model, paleoseismicity and paleostress analysis: Journal of South American Earth Sciences, v. 33/1, p. 110-118.

Fossa-Mancini, E., 1932, Faults in Comodoro Rivadavia oil field, Argentina: AAPG Bulletin, v. 16/6, p. 556-576.

Foster, M., and G. Iovine, 2008, Geometría y paleodrenaje regional de los sistemas de la Formación Castillo y Sección Tobácea, Cuenca del Golfo San Jorge: VII Congreso de Exploración y Desarrollo de Hidrocarburos, Trabajos Técnicos, p. 575-586.

Gawthorpe, R.L., and M. Leeder, 2000, Tectono-sedimentary evolution of active extensional basins: Basin Research, v. 12, p. 195-218.

Giacosa, R.E., J.M. Paredes, A. Nillni, M. Ledesma, and F. Colombo, 2004, Fallas normales de alto ángulo en el Neógeno del margen Atlántico de la Cuenca del Golfo San Jorge (46° S - 67° 30' O, Patagonia Argentina), *in* C. Viseras, J. Soria, and J. Fernández (Eds.), Avances recientes del conocimiento del Terciario: Boletín Geológico y Minero, Madrid, v. 115/3, p. 537-550.

Hechem, J.J., J.F. Homovc, and E.G. Figari, 1990, Estratigrafía del Chubutiano (Cretácico) en la Sierra de San Bernardo, cuenca del Golfo San Jorge, Argentina: 11th Congreso Geológico Argentino, San Juan, v. 3, p. 173-176.

Hechem J.J., and E.E. Strelkov, 2002, Secuencia sedimentaria mesozoica del Golfo San Jorge, *in* J.M. Haller (Ed.), Geología y Recursos Naturales de Santa Cruz: Relatorio del 15th Congreso Geológico Argentino, Buenos Aires, v. 1, p. 129-147.

Homovc, J.F., G.A. Conforto, P.A. Lafourcade, and L.A. Chelotti, 1995, Fold belt in the San Jorge Basin, Argentine: an example of tectonic inversion, *in* J.G. Buchanan, and P.G. Buchanan (Eds.), Basin Inversion: Geological Society Special Publication, v. 88, p. 235-248.

- Leeder, M.R., and R.L. Gawthorpe, 1987, Sedimentary models for extensional tilt-block/half graben basins, *in* M.P. Coward, J.F. Dewey, and P.L. Hancock (Eds.), Continental extensional tectonics: Geological Society of London, Special Publication 28, p. 139-152.
- Legarreta, L., M. Uliana, M. Torres, 1990, Secuencias deposicionales cenozoicas de Patagonia Central: sus relaciones con las asociaciones de mamíferos terrestres y episodios marinos epicontinentales: Actas del 3rd Simposio del Terciario de Chile, Concepción, p. 135-176.
- Legarreta, L., and M. Uliana, 1994, Asociaciones de fósiles y hiatos en el Supracretácico-Neógeno de Patagonia: una perspectiva estratigráfico-secuencial: Ameghiniana, v. 31/3, p. 257-281.
- Lesta, P., 1968, Estratigrafía de la Cuenca del Golfo San Jorge: 3rd Jornadas Geológicas Argentinas, Buenos Aires, v. 1, p. 251-280.
- Lesta, P., and R. Ferello, 1972, Región Extra-andina del Chubut y norte de Santa Cruz. En Geología Regional Argentina: Academia Nacional de Ciencias, Córdoba, p. 601-654.
- Lohr, T., C-M. Krawzyk, O. Oncken, and D.C. Tanner, 2008, Evolution of a fault surface from 3D attributes analysis and displacement measurements: Journal of Structural Geology, v. 30, p. 690-700.
- McLeod, A., J. Underhill, S. Davies, and N. Dawers, 2002, The influence of fault array evolution on synrift sedimentation patterns: Controls on deposition in the Strathspey-Brent-Stratfjord half graben, northern North Sea: AAPG Bulletin, v. 86, p. 1061-1093.
- Morley, C.K., 1999, How successful are analogue models in addressing the influence of pre-existing fabrics on rift structure?: Journal of Structural Geology, v. 21, p. 1267-1274.
- Morley, C.K., 2002a, Evolution of large normal faults: evidence from seismic reflection data: AAPG Bulletin, v. 86, p. 961-978.
- Morley, C.K., 2002b, Tectonic settings of continental extensional provinces and their impact on sedimentation and hydrocarbon prospectivity, *in* R. Renault and G. Ashley (Eds.), Sedimentation in Continental Rifts: SEPM Spec. Publ. 73, p. 25-55.
- Morley, C.K., N. Wonganan, A. Kornasawan, W. Phoosongsee, C. Haranya, and S. Pongwapee, 2004, Activation of rift oblique and rift parallel pre-existing fabrics during extension and their effect on deformation style: Examples from the rifts of Thailand: Journal of Structural Geology, v. 26, p. 1803-1829.
- Morley, C.K., R. King, R. Hillis, M. Tingay, and G. Backe, 2007, Deepwater fold and thrust belt classification, tectonics, structure and hydrocarbon prospectivity: A review: Earth-Science Reviews, v. 104, p. 41-91.
- Pankhurst, R.J., and C.W. Rapela, 1995, Production of Jurassic rhyolite by anatexis in the lower crust of Patagonia: Earth Planetary Science Letters, v. 134, p. 23-36.

Pankhurst, R.J., P.T. Leat, P. Sruoga, C.W. Rapela, M. Marquez, B.C. Storey, and T.R. Riley, 1998, The Chon Aike province of Patagonia and related rocks in West Antarctica: A silicic large igneous province: *Journal of Volcanology and Geothermal Research*, v. 81, p. 113-136.

Paredes, J.M., 2009, Sedimentary Evolution of the Golfo San Jorge Basin, Central Patagonia, Argentina, *in* L.M. Ibañez, M.S. Moyano, and G.F. Aceñolaza (Eds.), *Argentinean Fluvial Basins: Ancient and present day examples: Excursion Guide Book*, 9th International Conference on Fluvial Sedimentology, San Miguel de Tucumán, Basin Analysis Series I, p. 187-275.

Paredes, J.M., S. Plazibat, C. Crovetto, J. Stein, E. Cayo, and A. Schiuma, 2013, Fault kinematics and depocenter evolution of oil-bearing, continental successions of the Mina del Carmen Formation (Albian) in the Golfo San Jorge basin, Argentina: *Journal of South American Earth Sciences*, v. 46, p. 63-79.

Partyka, G., J. Gridley, J.A. Lopez, 1999, Interpretational applications of spectral decomposition in reservoir characterization: *The Leading Edge*, v. 18, p. 353-360.

Prosser, S., 1993, Rift-related linked depositional systems and their seismic expression, *in* G.D. Williams, A. Dobb (Eds.), *Tectonics and Seismic Sequence Stratigraphy: Geological Society Special Publication*, v. 71, p. 35-66.

Rodriguez, J.F.R., 1992, Interpretación paleoambiental de la Formación Bajo Barreal (Cretácico tardío) en Estancia Ocho Hermanos, Chubut: 4th Reunión Argentina de Sedimentología, La Plata, v. 2, p. 81-88.

Scazzioti, F., 2008, El factor estratigráfico presente en la formación Mina El Carmen, flanco norte de la cuenca del Golfo San Jorge: 7th Congreso de Exploración y Desarrollo de Hidrocarburos, Trabajos Técnicos, Mar del Plata, p. 101-117.

Schiuma, A., C. Crovetto, D. Álvarez, J. Gómez, D. Andersen, L. Alonso, López O. Alvarado, A. Rasgido, 2013, Revitalización del Yacimiento Koluel Kaike (Santa Cruz) mediante el desarrollo de reservorios de la FM. Mina del Carmen: V Congreso de Producción y Desarrollo de Reservas de Hidrocarburos, Trabajos Técnicos en CD. Rosario.

Sciutto, J.C., 1981, Geología del Codo del Río Senguerr, Chubut, Argentina: 8th Congreso Geológico Argentino, San Luis, v. 3, p. 203-219.

Sylwan, C., 2001, Geology of the Golfo San Jorge Basin, Argentina: *Geología de la Cuenca del Golfo San Jorge, Argentina: Journal of Iberian Geology*, v. 27, p. 123-157.

Uliana, M.A., and K.T. Biddle, 1987, Permian to Late Cenozoic evolution of Northern Patagonia: main tectonic events, magmatic activity and depositional trends, *in* Gondwana Six: structure, tectonics and geophysics: American Geophysical Union, Geophysical Monograph 40, v. 271-286.

- Uliana, M.A., K.T. Biddle, and J. Cerdán, 1989, Mesozoic Extension and the Formation of Argentine Sedimentary Basins, *in* A.J. Tankard and H.R. Balkwill (Eds.), *Extensional deformation and Stratigraphy of the North Atlantic margins: AAPG Memoir 46*, p. 599-614.
- Umazano, A.M., E. Bellosi, G. Visconti, R. Melchor, 2008, Mechanism of aggradation in fluvial systems influenced by explosive volcanism: An example from the Upper Cretaceous Bajo Barreal Formation, San Jorge Basin, Argentina: *Sedimentary Geology*, v. 203, p. 213-228.
- Willemse, E.J.M., D.D. Pollard, and A. Aydin, 1996, Three-dimensional analyses of slip distributions on normal fault arrays with consequences for fault scaling: *Journal of Structural Geology*, v. 18, p. 295-309.

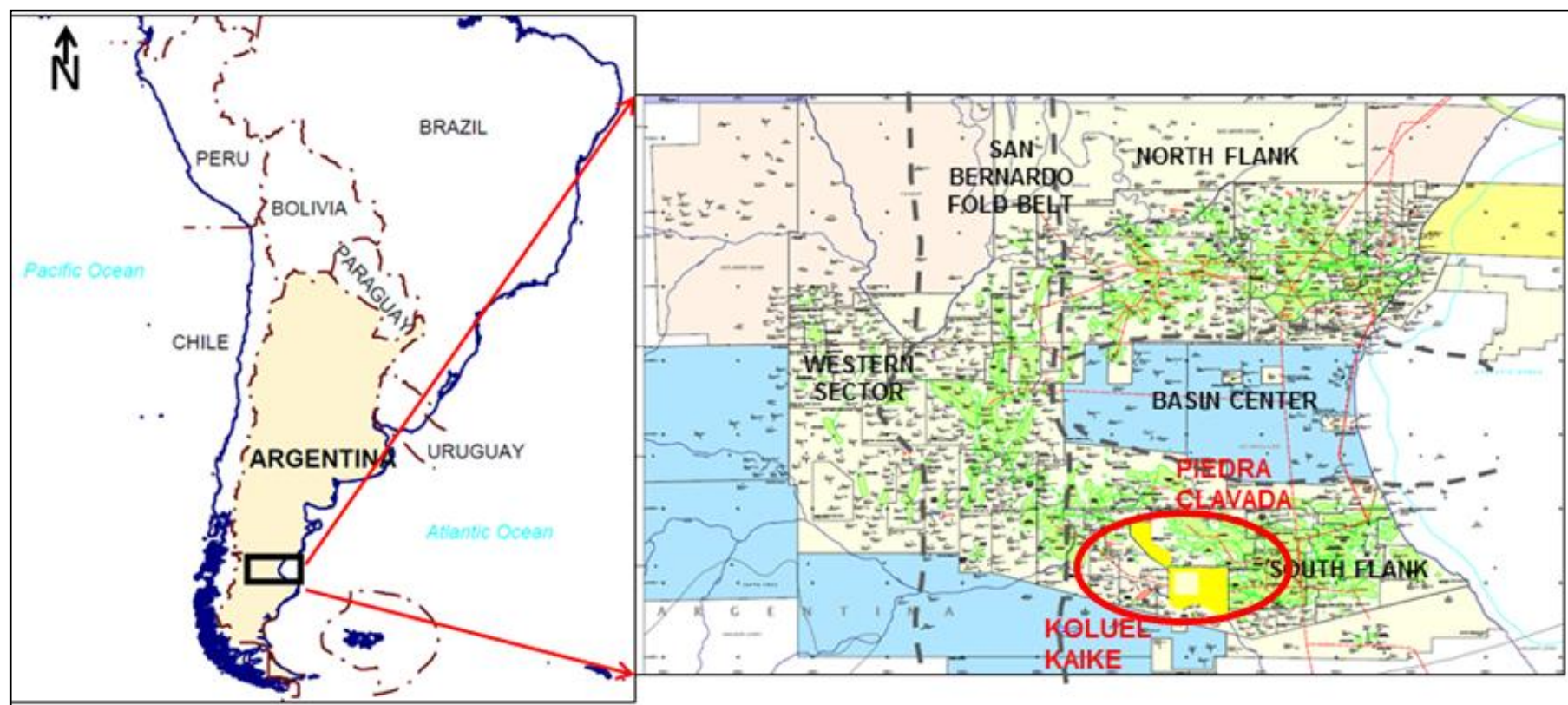


Figure 1. (A) Location of Piedra Clavada and Koluel Kaike fields in Cuenca del Golfo San Jorge Basin, Argentina.

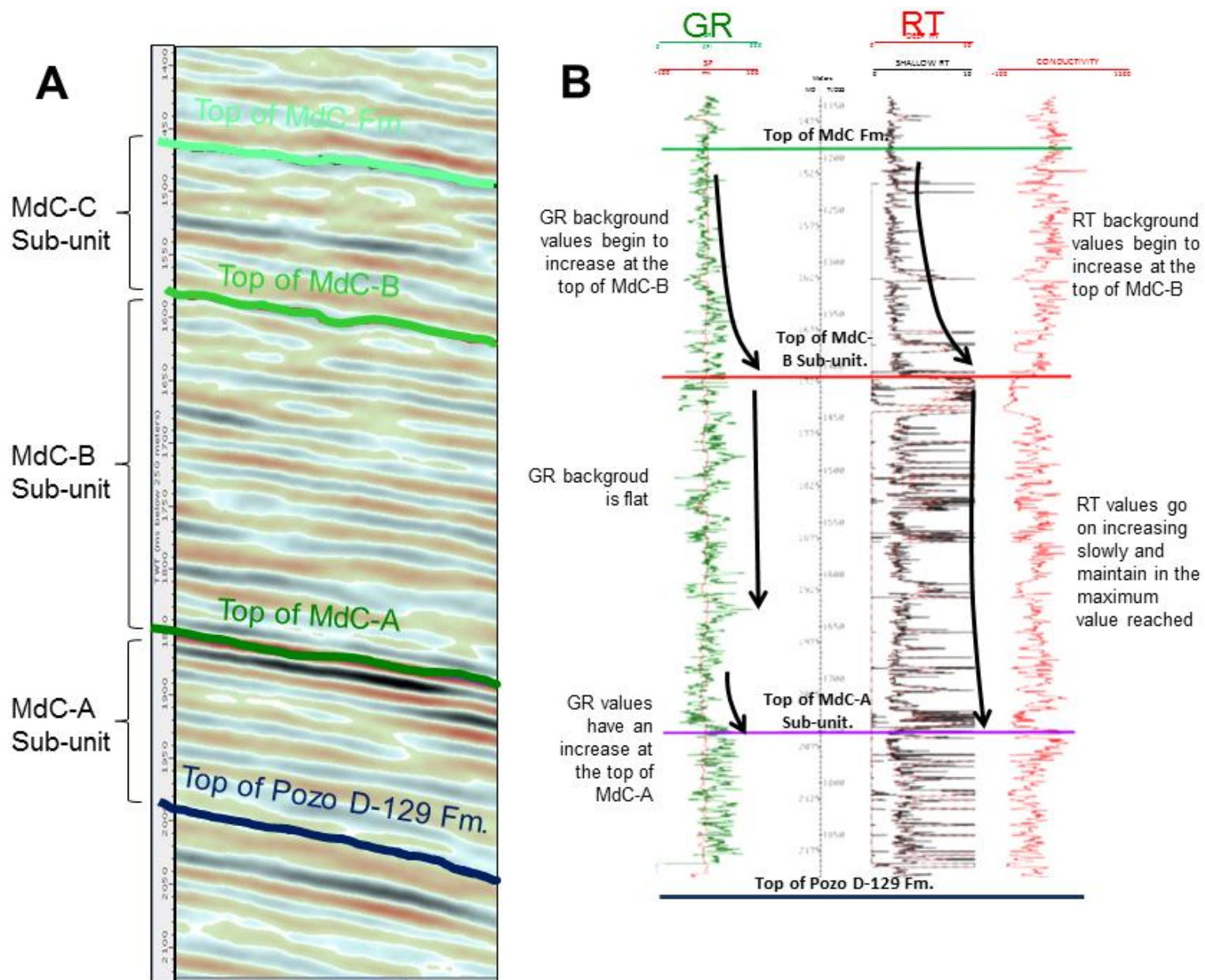


Figure 3. (A) Seismic division of Mina del Carmen Formation. (B) Well-log division of Mina del Carmen Formation. GR: gamma ray log. RT: resistivity log.

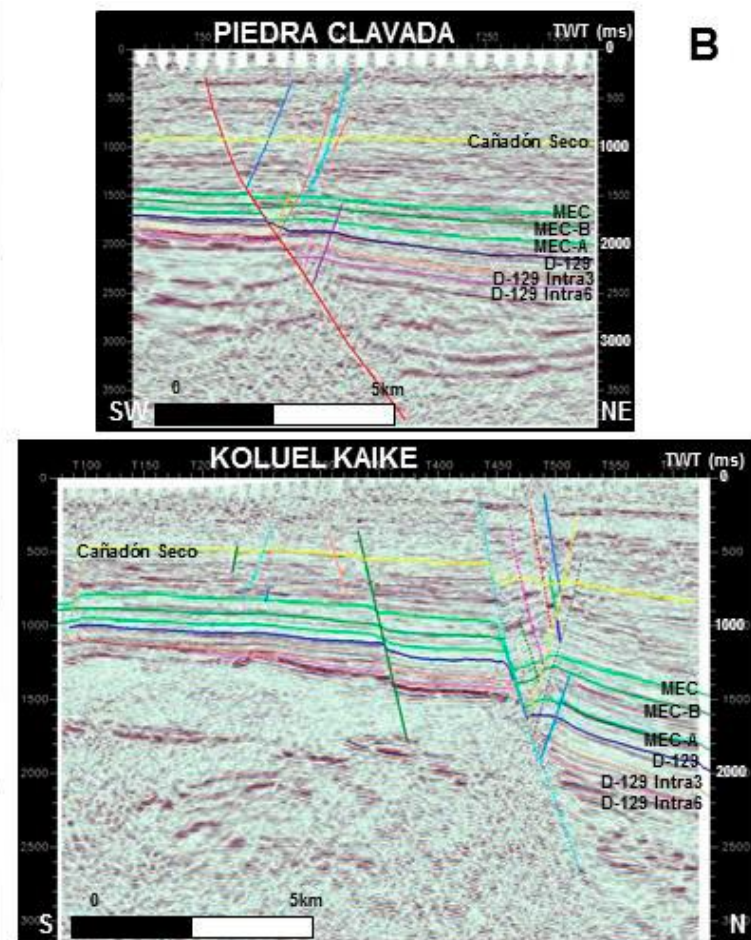
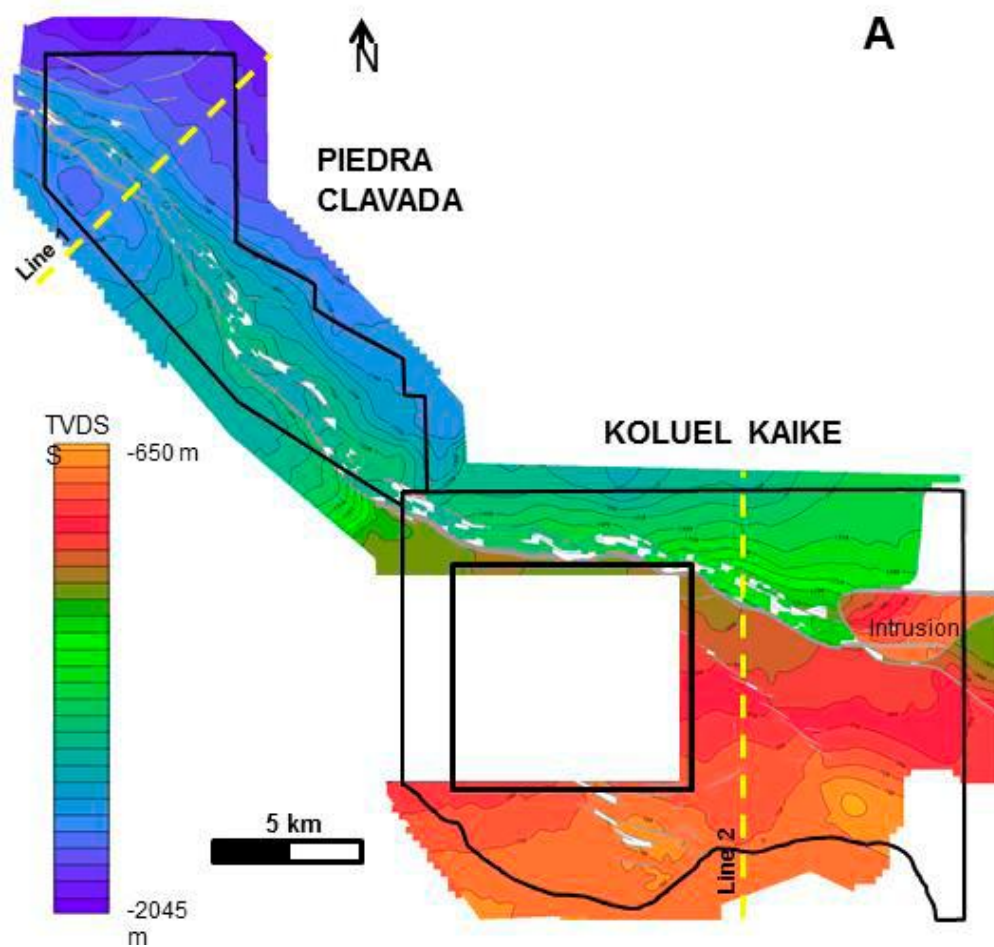


Figure 4. (A) Structural map at Top of Mina del Carmen Formation. Depths below sea level. Equidistance: 50 m. (B) Seismic lines showing the structure in Koluel Kaike and in Piedra Clavada. Line positions are indicated on the map.

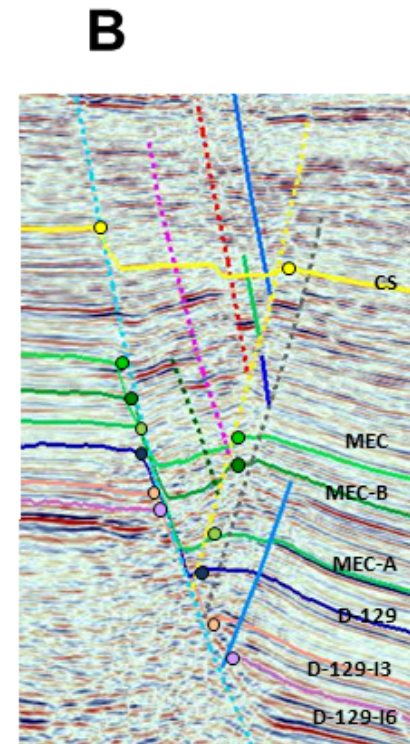
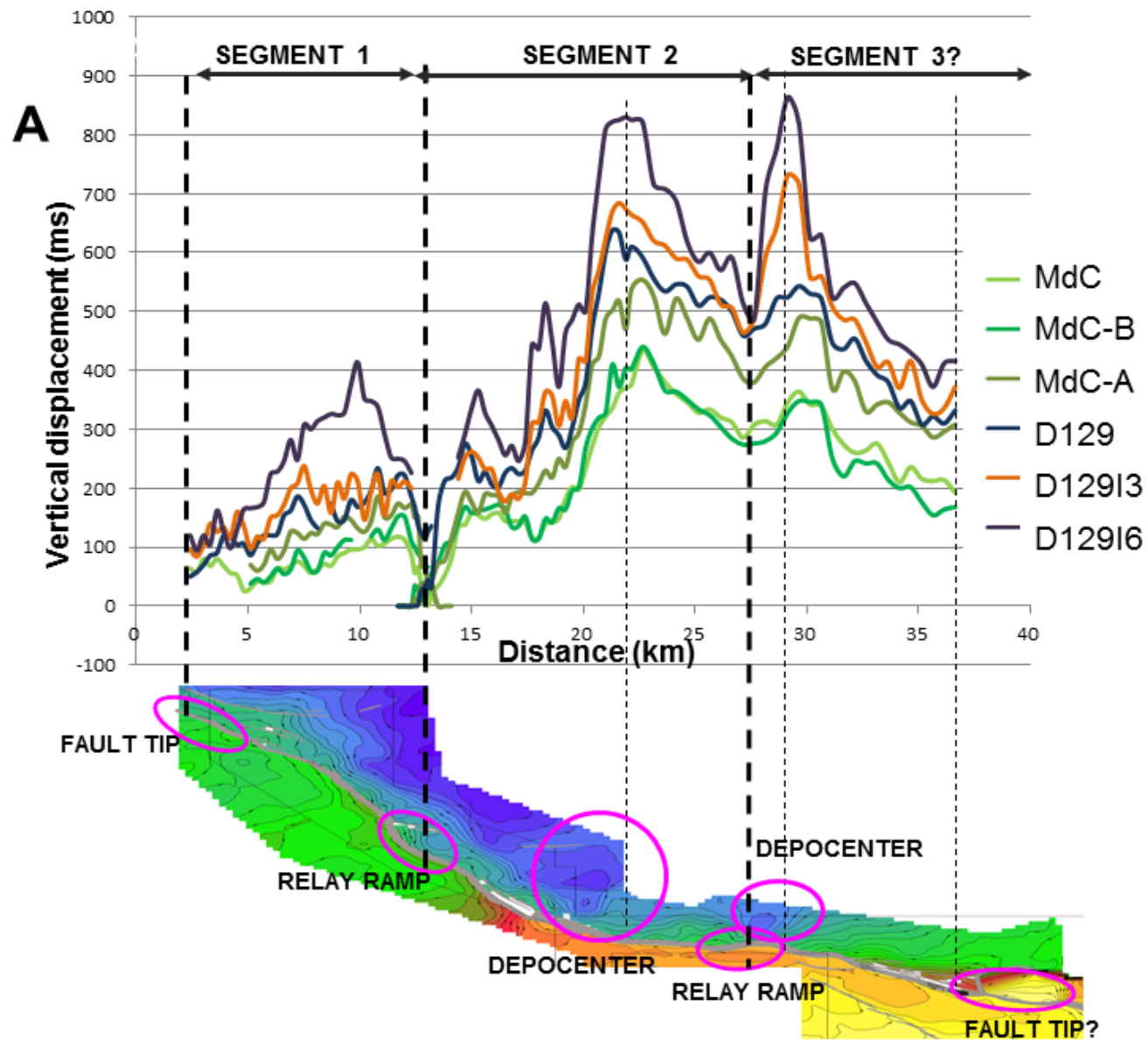


Figure 5. (A) Displacement plot for the principal fault in Piedra Clavada and Koluel Kaike fields. Isochoric map of Mina del Carmen Formation is shown on the bottom of the figure. (B) Seismic line showing the place where times were computed for each horizon.

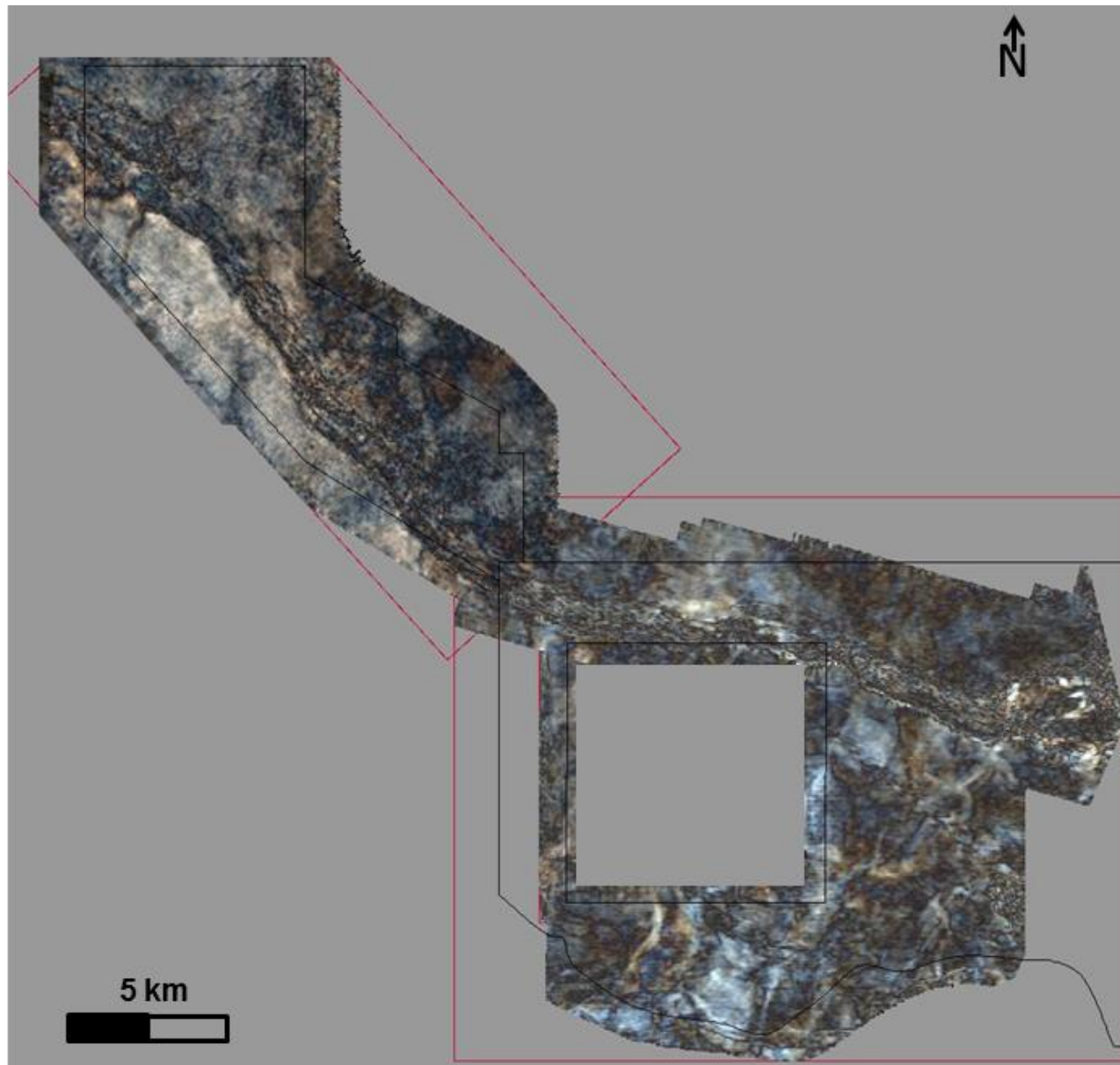


Figure 6. Seismic spectral decomposition at top of Mina del Carmen Formation. RGB blending of 20+25+30 Hz frequencies.

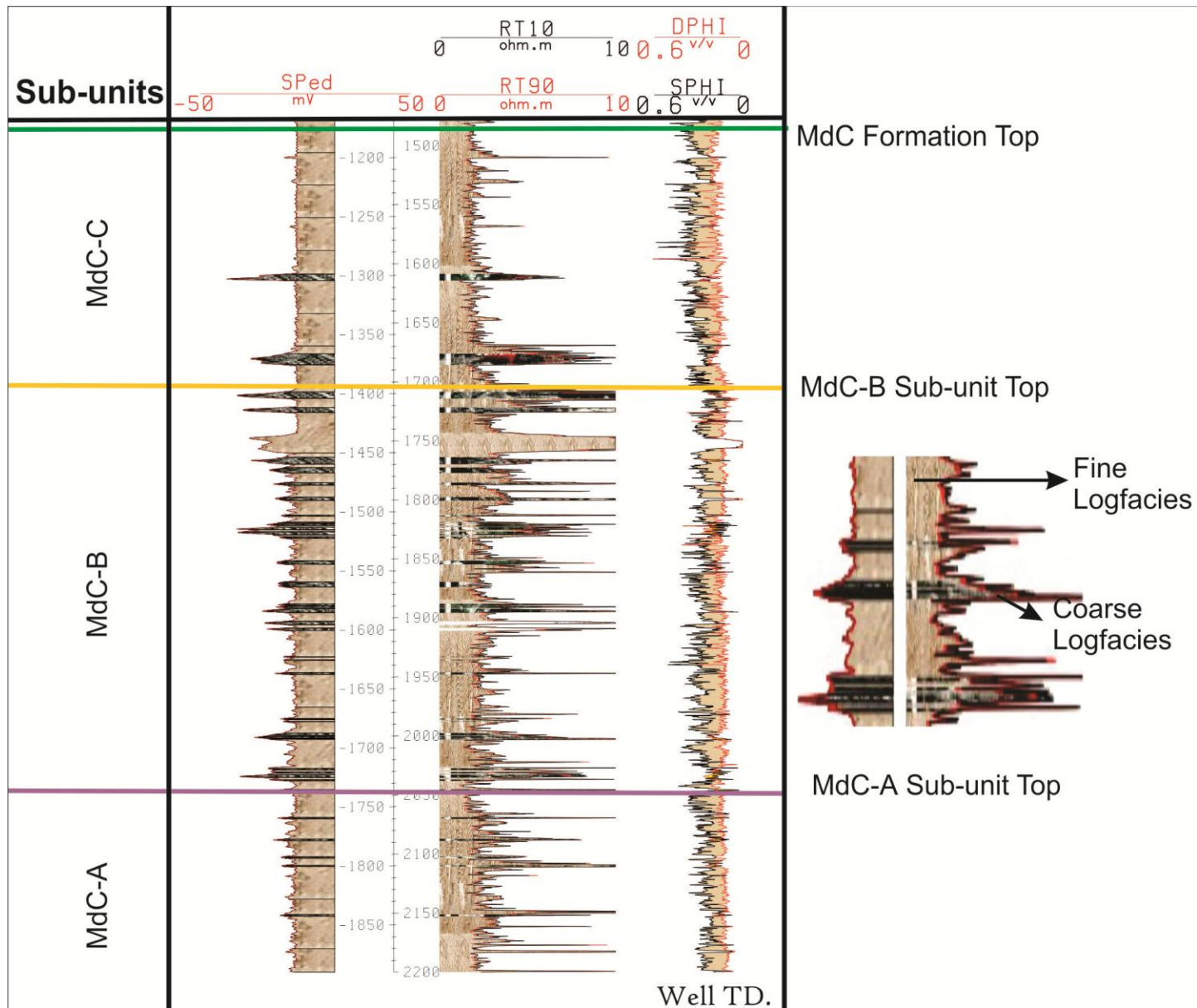


Figure 7. Logfacies identified in a well log of the hanging wall. Detail of coarse and fine logfacies. SPed: spontaneous potential log. RT10/RT90: shallow/deep resistivity logs. DPHI: porosity derived from density log. SPHI: porosity derived from sonic log.

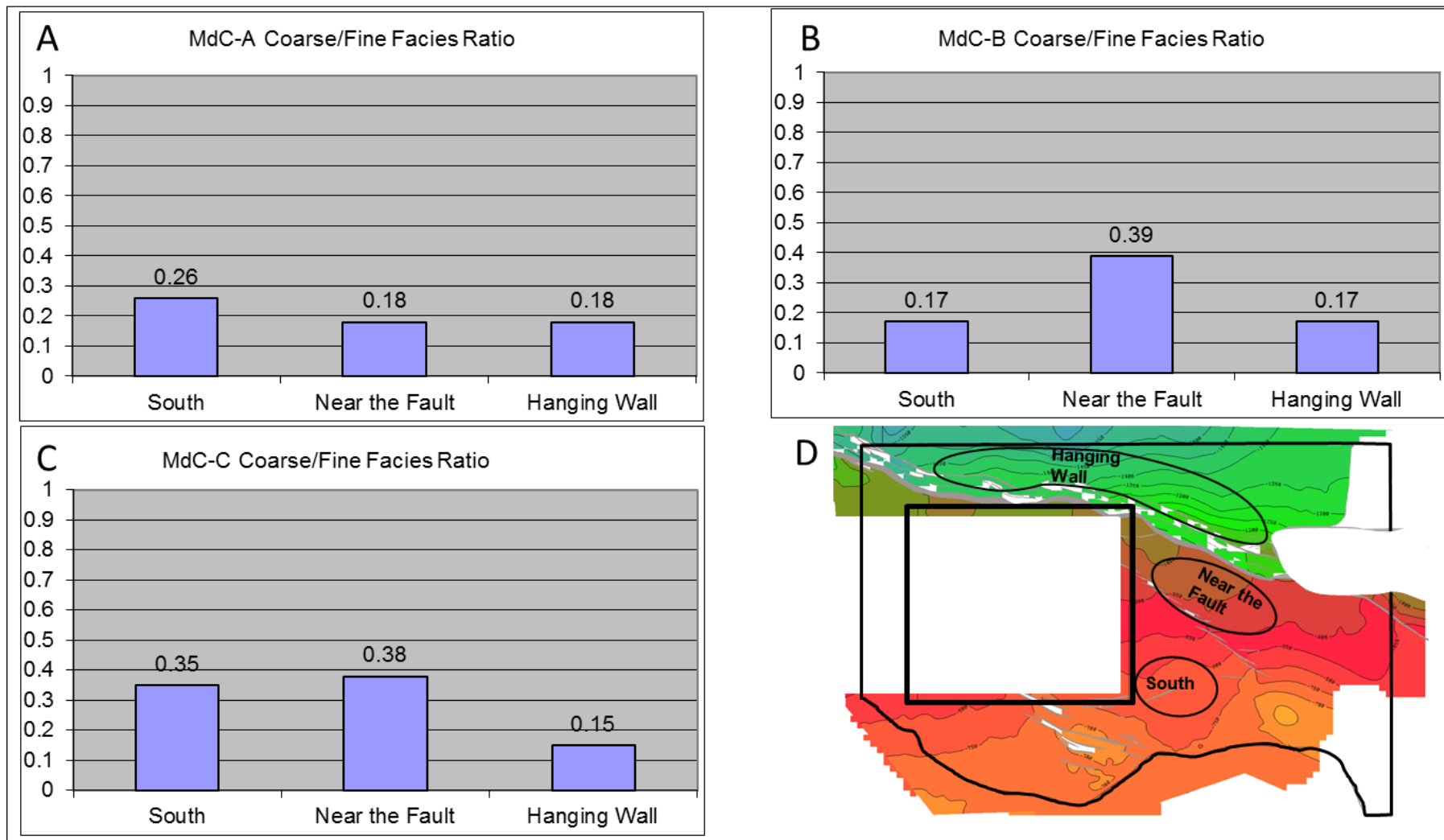


Figure 8. Logfacies ratio distribution in Koluel Kaike Field. (A) MdC-A Sub-unit. (B) MdC-B Sub-unit. (C) MdC-C Sub-unit. (D) Schematic map showing areas location.

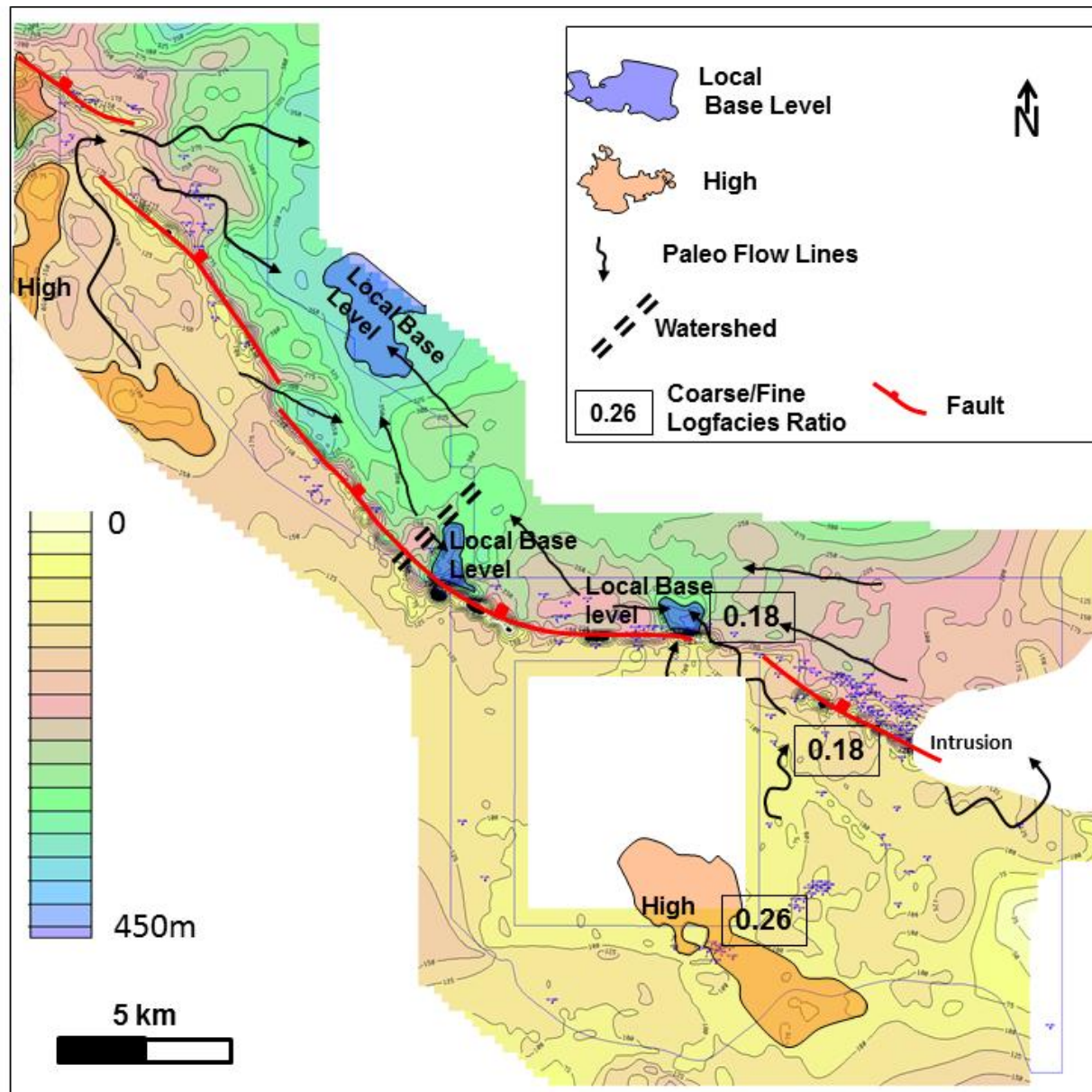


Figure 9. Isochoric map of MdC-A sub-unit, showing logfacies ratios and interpreted paleo-flow directions. Equidistance: 25 m.

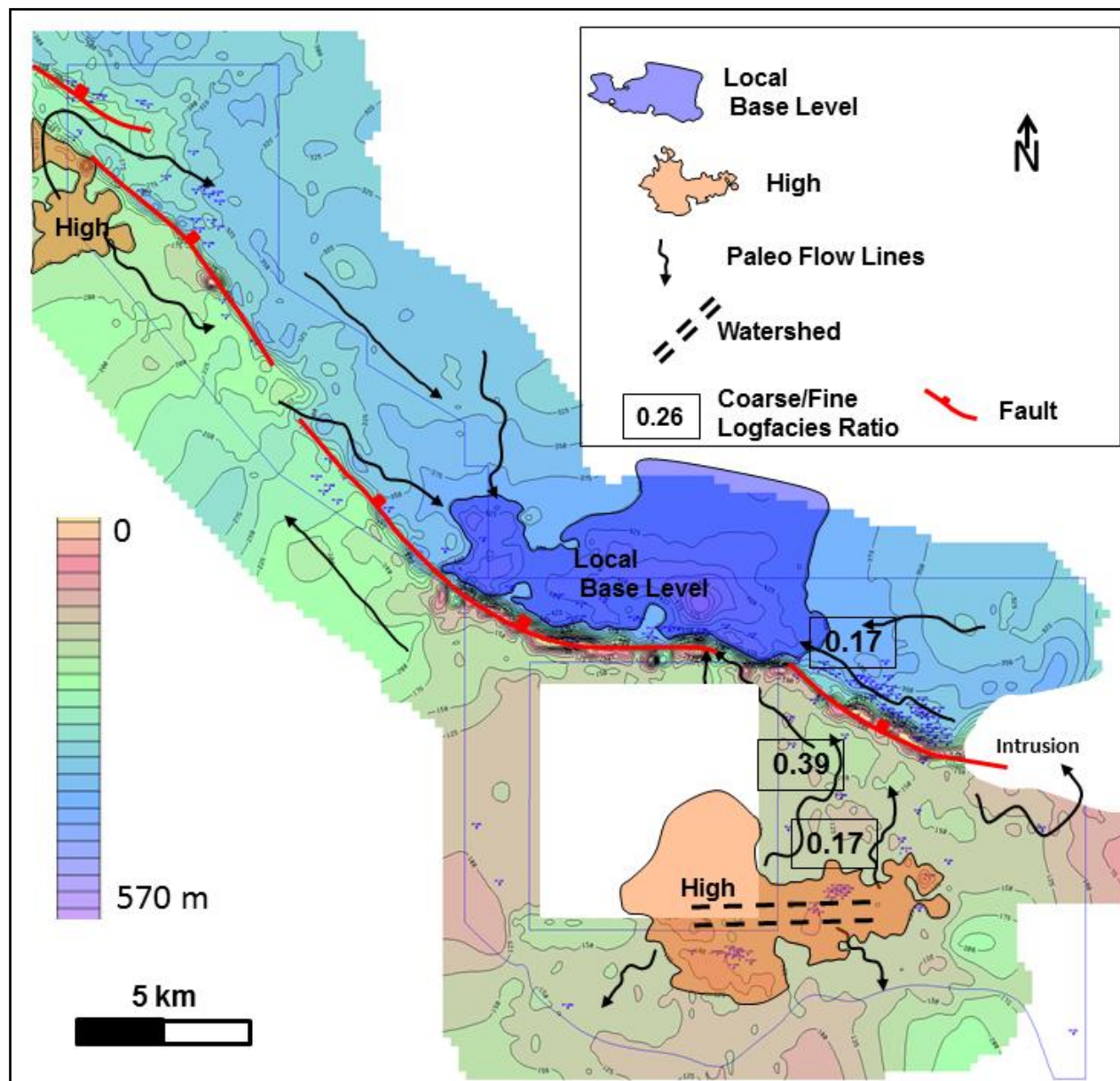


Figure 10. Isochoric map of MdC-B sub-unit, showing logfacies ratios and interpreted paleo-flow directions. Equidistance: 25 m.

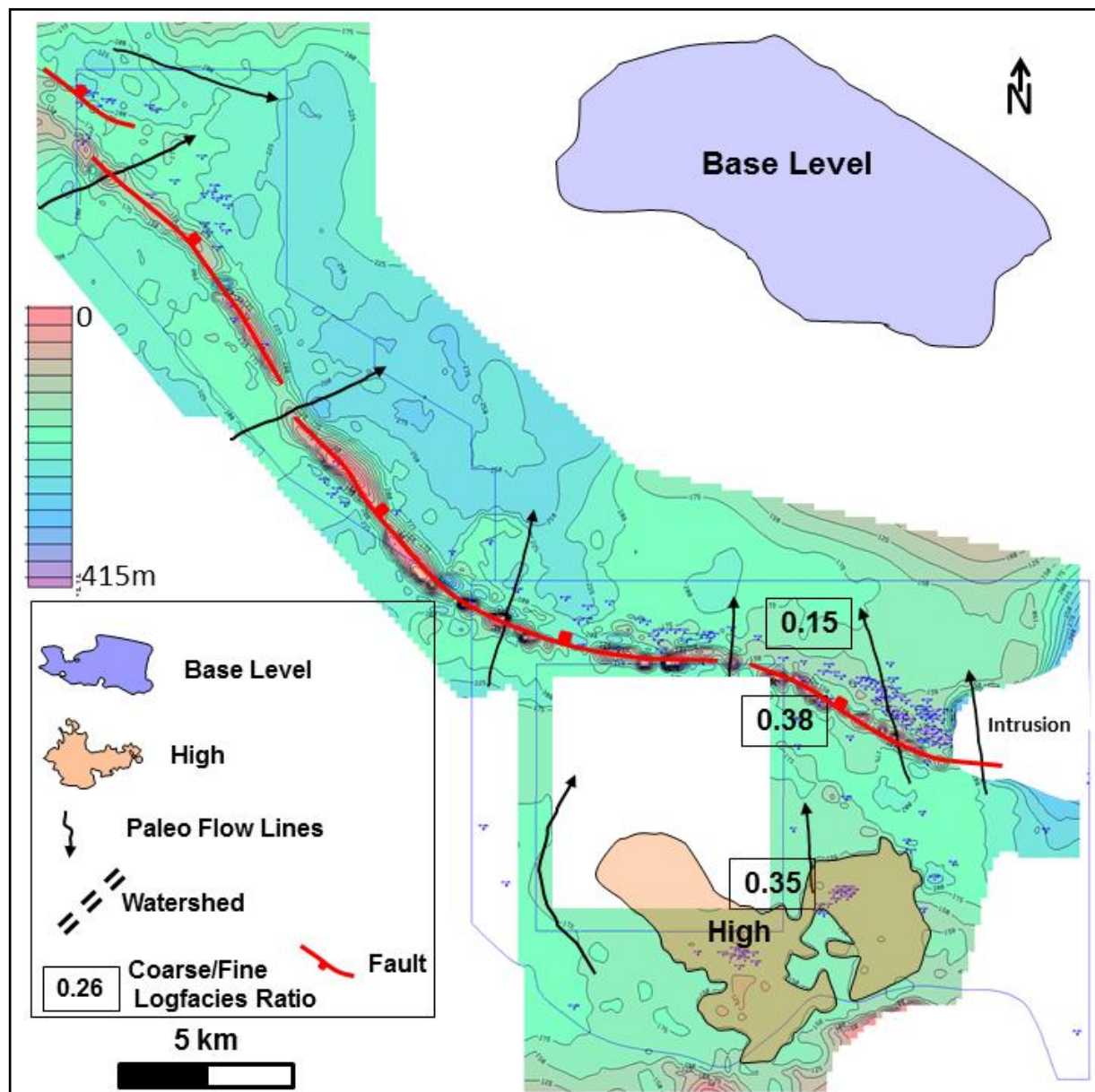


Figure 11. Isochoric map of MdC-C sub-unit, showing logfacies ratios and interpreted paleo-flow directions. Equidistance: 25 m.